PATTERN SOLUTIONS OF THE KLAUSMEIER MODEL FOR BANDED VEGETATION IN SEMIARID ENVIRONMENTS V: THE TRANSITION FROM PATTERNS TO DESERT

Author(s): JONATHAN A. SHERRATT

Source: *SIAM Journal on Applied Mathematics*, Vol. 73, No. 4 (2013), pp. 1347-1367
Published by: Society for Industrial and Applied Mathematics
Stable URL: https://www.jstor.org/stable/24510684
Accessed: 16-05-2024 11:44 +00:00

SIAM J. APPL. MATH.
Vol. 73, No. 4, pp. 1347–1367

PATTERN SOLUTIONS OF THE KLAUSMEIER MODEL FOR BANDED VEGETATION IN SEMIARID ENVIRONMENTS V: THE TRANSITION FROM PATTERNS TO DESERT*

JONATHAN A. SHERRATT†

Abstract. Vegetation in semideserts often self-organizes into spatial patterns. On gentle slopes, these typically consist of stripes of vegetation running parallel to the contours, separated by stripes of bare ground. The Klausmeier model is one of the oldest and most established of a number of mathematical models for this "banded vegetation." The model is a system of reaction-diffusion-advection equations. Under the standard nondimensionalization, one of its dimensionless parameters (ν) reflects the relative rates of water flow downhill and plant dispersal and is therefore very large. This paper is the fifth and last in a series in which the author provides a detailed analytical understanding of the existence and form of pattern solutions (periodic travelling waves) of the Klausmeier model, to leading order as $\nu \to \infty$. The problem is a very rich one because the underlying mathematics depends fundamentally on the way in which the migration speed c scales with ν. This paper concerns the case $1 = O(c)$ and $c = o(\nu^{1/2})$ as $\nu \to \infty$. The author derives leading order expressions for the curves bounding the parameter region giving patterns, and for the pattern forms in this region. An important consequence of this is leading order formulae for the maximum and minimum rainfall levels for which patterns exist. The author demonstrates via numerical simulations that a decrease in rainfall through the minimum level for patterns causes a transition to full-blown desert that cannot be reversed by increasing the rainfall again.

Key words. pattern formation, arid landscapes, reaction-diffusion-advection, WAVETRAIN, tiger bush, desertification

AMS subject classifications. 92D40, 35C07, 35M10

DOI. 10.1137/120899510

1. Introduction.

In semiarid environments, the infiltration rate of rainwater into the soil increases with vegetation density [1, 2]. This is due both to increased levels of organic matter in the soil and to the presence of root networks. Since water is a limiting resource in these ecosystems, there is an adaptive benefit to plants of forming localized aggregations rather than having more sparse uniform distributions. Consequently spatial patterns of vegetation are widespread in many semiarid regions [3, 4, 5]. The most striking manifestation of such patterns is the "banded vegetation" that occurs on gentle slopes, in which stripes of vegetation run parallel to the contours, separated by stripes of bare ground. This has been documented in many parts of the world, particularly Australia [6], Southwestern North America [7], and Africa [8].

The "water redistribution hypothesis" for banded vegetation argues that rain falling on bare ground infiltrates only a little, mostly running off in the downhill direction to the next vegetation band. Here it infiltrates into the soil, thereby facilitating plant growth. One implication of this argument is that moisture levels should be higher on the uphill edge of the bands than on their downhill edge, and this is widely observed, being reflected in lower levels of plant death and higher seedling densities [9, 10]. Therefore one expects vegetation bands to move uphill on a timescale of the plant generation time, as new vegetation grows immediately upslope of the bands,

*Received by the editors November 9, 2012; accepted for publication (in revised form) April 17, 2013; published electronically July 3, 2013.
http://www.siam.org/journals/siap/73-4/89951.html

†Department of Mathematics and Maxwell Institute for Mathematical Sciences, Heriot-Watt University, Edinburgh EH14 4AS, UK (j.a.sherratt@hw.ac.uk).

with a corresponding loss of biomass through plant death at the downslope edge. Such movement is indeed observed in many cases [11], [4, Table 5]. However, some field studies also report stationary banded patterns [6, 8, 11]. This has been attributed to complicating factors including inhibition of seed germination by long-term changes in soil structure in nonvegetated regions [6], and preferential dispersal of seeds in the downslope direction due to transport in run-off [12, 13].

This paper concerns a mathematical model for banded vegetation due to Klausmeier [14] that is based on the water redistribution hypothesis. However, it is important to comment that other mechanisms for banded vegetation have been proposed. In particular the extensive root systems that occur in semiarid regions [15] lead to nonlocality in water uptake, and some authors have argued that this plays an important role in the pattern formation process, either alongside the water redistribution mechanism [16, 17] or in combination with short-range facilitation due to shading [18, 19].

When suitably nondimensionalized [14, 20], the Klausmeier model is

$$\partial u/\partial t = \overbrace{wu^2}^{\text{plant growth}} - \overbrace{Bu}^{\text{plant loss}} + \overbrace{\partial^2 u/\partial x^2}^{\text{plant dispersal}}, \tag{1.1a}$$

$$\partial w/\partial t = \underbrace{A}_{\text{rainfall}} - \underbrace{w}_{\text{evaporation}} - \underbrace{wu^2}_{\text{uptake by plants}} + \underbrace{\nu \partial w/\partial x}_{\text{flow downhill}}. \tag{1.1b}$$

Here $u(x,t)$ is plant density, $w(x,t)$ is water density, t is time, and x is a one-dimensional space variable running in the uphill direction. The dimensionless parameters A, B, and ν can be most usefully interpreted as reflecting rainfall, plant loss, and slope gradient, respectively, although they actually represent a combination of ecological quantities. Klausmeier's [14] parameter estimates were $A = 0.9$–2.8, $B = 0.45$ for grass and $A = 0.08$–0.2, $B = 0.045$ for trees, with $\nu = 182.5$. The parameter ν is large because it reflects the relative rates of water flow downhill and of plant dispersal [14, 20]. Note that wu^2 is the only nonlinear term in (1.1); it assumes that the infiltration rate is proportional to vegetation density, which is consistent with the available data (e.g., [2, Figure 4]).

Equations (1.1) have either one or three spatially homogeneous steady states. The "desert" state $(0, A)$ is always a locally stable steady state. For $A \geq 2B$, $(u_\pm, w_\pm) = \left(\left[A \pm \sqrt{A^2 - 4B^2}\right]/2B, \left[A \mp \sqrt{A^2 - 4B^2}\right]/2\right)$ are also solutions. (u_-, w_-) is unstable, but the stability of (u_+, w_+) is parameter dependent. Provided that $B < 2$, (u_+, w_+) is locally stable to spatially homogeneous perturbations; $B < 2$ is an ecologically realistic assumption that I will make throughout this paper. However, there is a range of values of the rainfall parameter A (to be discussed in this paper) in which (u_+, w_+) is unstable to inhomogeneous perturbations, and in which (1.1) has spatial patterns. Figure 1.1 illustrates a typical example of such a pattern. There are alternating peaks and troughs of vegetation density, corresponding respectively to vegetation bands and the bare interbands, and there is a corresponding pattern of water density. The patterns move at a constant speed in the positive x direction, corresponding to the uphill migration seen in many data sets and discussed above.

The Klausmeier model (1.1) was the first of many continuous models for banded vegetation formation based on the water redistribution hypothesis. Most of the subsequent models represent soil and surface water separately (e.g., [21, 22, 23]), and some authors have also extended their models to include herbivory [24] and variations in rainfall [25, 26, 27]. However, almost all of these studies use only numerical simula-

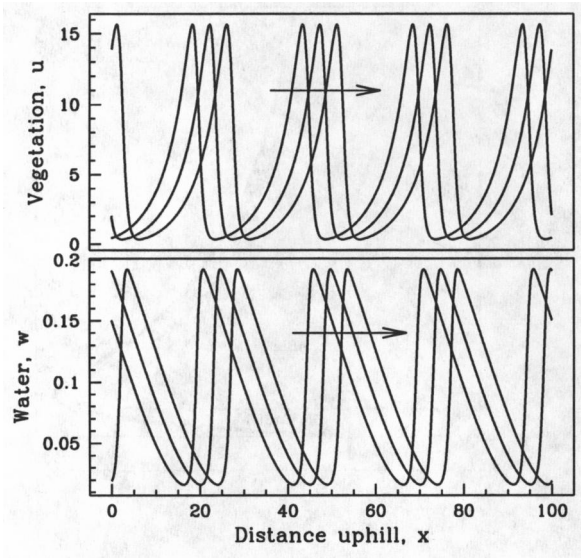

FIG. 1.1. *A typical example of a pattern solution of the model* (1.1) *for vegetation in semiarid environments. The alternating peaks and troughs of u correspond to vegetation bands and the gaps between them, respectively. The initial conditions are small random perturbations (amplitude ±5%) to the vegetated steady state* (u_+, w_+), *and the solutions are plotted at* $t = 2000$, 2003, *and* 2006 *dimensionless time units, illustrating the uphill migration of the patterns. The long initial time ensures that transients have decayed. The parameter values are* $A = 2.2$, $B = 0.45$, *and* $\nu = 182.5$. *The spatial domain is of length* 100 *with periodic boundary conditions. The equations were solved numerically using a semi-implicit finite difference method with time step* $\delta t = 1.1 \times 10^{-4}$ *and uniform spatial grid spacing* $\delta x = 0.025$; *these give the CFL number* $\nu \delta t / \delta x = 0.8$.

tions of the model equations; one recent exception is a proof by Goto et al. [28] of the existence of solutions for the model of Gilad et al. [16]. This paper is the fifth and last in a series in which I attempt a comprehensive analytical study of the Klausmeier model (1.1). My approach exploits the large value of the slope parameter ν, and I investigate the asymptotic form of pattern solutions as $\nu \to \infty$. I assume formal expansions for the pattern solutions; a possible area for future work would be to establish rigorous results using geometric singular perturbation theory [29, 30]. The problem is a very rich one because the underlying mathematics depends fundamentally on the way in which the migration speed c scales with ν. Previously I have considered the cases $c \gg \nu^{1/2}$ [31, 32], $c = O_s(\nu^{1/2})$ [33], and $c \ll 1$ [34] as $\nu \to \infty$. Note that the notation $f = O_s(g)$ denotes $f = O(g)$ and $f \neq o(g)$. In this paper I consider the remaining case of $1 = O(c)$ and $c = o(\nu^{1/2})$. This is a particularly important parameter region because it includes the minimum level of rainfall giving patterns, below which the model (1.1) predicts vegetation-free desert as the only possible state.

Since they move at a constant speed and with constant shape, pattern solutions of (1.1) are periodic traveling waves, with the form $u(x,t) = U(z)$, $w(x,t) = W(z)$, $z = x - ct$. Here $c > 0$ is the migration speed in the uphill direction. Substituting these forms into (1.1) gives

$$d^2U/dz^2 + c\,dU/dz + WU^2 - BU = 0, \tag{1.2a}$$

$$(\nu + c)dW/dz + A - W - WU^2 = 0. \tag{1.2b}$$

A detailed numerical study of the existence and stability of periodic traveling waves is possible via numerical continuation; for this I have used the software package WAVE-

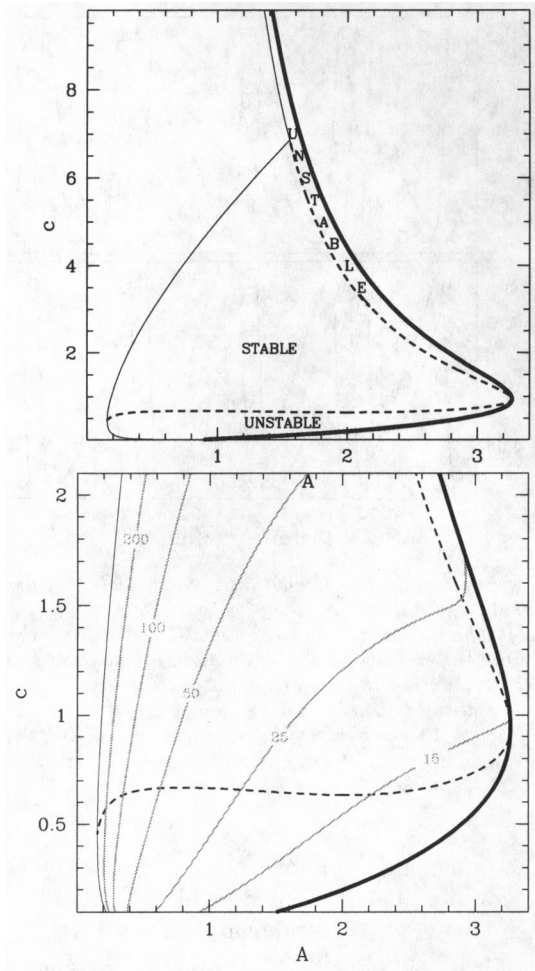

FIG. 1.2. *Existence and stability of pattern solutions of* (1.1) *for* $B = 0.45$ *and* $c = 182.5$. *Patterns exist in between the locus of Hopf bifurcation points of* $(U, W) = (u_+, w_+)$ *for* (1.2) *(thick solid black line) and the locus of homoclinic solutions (thin solid black line). The dashed black line is the boundary between patterns that are stable or unstable as solutions of* (1.1). *Top: A wider range of* c *values, although it has been truncated at* $c \approx 10$*; the parameter region giving patterns actually extends up to* $c \approx 50$ [32]. *Bottom: A close-up of the part of the parameter plane studied in this paper, including contours along which the pattern period (wavelength) is constant at the value indicated (grey lines). For* c *between about* 0.002 *and* 0.004, *and also for* c *above about* 14, *there is a fold in the branch of pattern solutions, with small regions of parameter space in which there are two different patterns (both unstable) for given* A *and* c *(see* [32, 34] *for details). In the remainder of the parameter plane there is at most one pattern solution. All calculations and plotting were done using the software package* WAVETRAIN [35, 36, 37, 38]. *Full details of the* WAVETRAIN *input files, run commands (including run times), and plot commands are given at* http://www.ma.hw.ac.uk/~jas/supplements/kl5.

TRAIN [35, 36]. A typical result is illustrated in Figure 1.2(top), which shows the region of the A–c parameter plane in which patterns exist and also the part of that region in which they are stable as solutions of (1.1). The pattern region is bounded to the right by a locus of Hopf bifurcations of (u_+, w_+) in (1.2), and to the left by a locus of homoclinic solutions. Figure 1.2(bottom) shows a close-up of the part of parameter space that is the subject of this paper, with contours of constant pattern wavelength superimposed on the plot. The basic objective of this paper is to determine asymptotic

expansions as $\nu \to \infty$ for the loci of Hopf bifurcations and homoclinic solutions that bound the pattern region, and for the form of the patterns for parameters between these loci.

In section 2 I consider pattern solutions at rainfall levels close to the maximum possible value when $c = O_s(1)$. Section 3 is concerned with the form of solutions in the interior of the region of parameter space giving patterns, and section 4 focuses on patterns at the lowest possible rainfall levels, with c assumed to be $O_s(1)$ in both cases. A key result of section 4 is the asymptotic form of the minimum rainfall giving patterns; as A is decreased through this value, there is a transition to total desert. In section 5 I describe numerical simulations of this transition. In section 6 I consider patterns with $1 \ll c \ll \nu^{1/2}$. I conclude (section 7) with a discussion of the stability of pattern solutions.

2. Pattern solutions for $c = O_s(1)$, $A = O_s(\nu^{1/2})$. Although my previous paper [34] was concerned primarily with the case $c = o(1)$ as $\nu \to \infty$, it also included a brief discussion of patterns when $c = O_s(1)$ and $A = O_s(\nu^{1/2})$; this scaling includes part of the Hopf bifurcation locus. In this section I briefly summarize this previous work and then present some extensions. My key conclusion is that there is exactly one pattern at every point in this part of the A–c plane to the left of a locus of Hopf bifurcation points whose form can be calculated explicitly. I will also show that the pattern wavelength varies nonmonotonically with c and A in this parameter region.

For $c = O_s(1)$ and $A = O_s(\nu^{1/2})$ the traveling wave equations (1.2) can be simplified by the rescalings $\check{U} = (B/A)U$, $\check{W} = (A/B^2)W$, $\check{z} = B^{1/2}z$, $\check{c} = B^{-1/2}c$, $\Gamma = A^2/(\nu B^{5/2})$. Note that $\Gamma = O_s(1)$ as $\nu \to \infty$. In terms of these new variables the leading order form of (1.2) as $\nu \to \infty$ is

$$d^2\check{U}/d\check{z}^2 + \check{c}\,d\check{U}/d\check{z} + \check{W}\check{U}^2 - \check{U} = 0, \tag{2.1a}$$

$$d\check{W}/d\check{z} + \Gamma\left(1 - \check{W}\check{U}^2\right) = 0. \tag{2.1b}$$

My rescalings map $(U, W) = (u_+, w_+)$ and (u_-, w_-) to $(\check{U}, \check{W}) = (1, 1)$ and $(0, \infty)$, respectively. Calculation of the eigenvalues of (2.1) at $(1, 1)$ shows that there is a Hopf bifurcation at $\Gamma = \Gamma_H \equiv (\check{c}^2 + 2 - \sqrt{\check{c}^4 + 4})/(2\check{c})$ [34]. This Hopf bifurcation locus is illustrated in Figure 2.1. It has a turning point at $A = (\sqrt{2}-1)^{1/2}B^{5/4}\nu^{1/2} \approx 0.6436B^{5/4}\nu^{1/2}$, which is a Turing bifurcation point for (1.1).

In [34] I proved that for all values of $\check{c}$ the Hopf bifurcation at $\Gamma = \Gamma_H$ is subcritical, meaning that the branch of pattern (limit cycle) solutions leaves in the direction of decreasing Γ. Moreover, numerical continuation suggests that the pattern solution branches remain monotonic in Γ away from the Hopf bifurcation locus. Such monotonicity implies exactly one pattern solution at all points in the Γ–$\check{c}$ plane to the left of the Hopf bifurcation locus $\Gamma = \Gamma_H$. Figure 2.2 illustrates these solution branches for three different values of Γ, plotting the period (pattern wavelength) as a function of $\check{c}$. One notable feature of these plots is that for the two smaller Γ values there is a local maximum in the period as a function of $\check{c}$, while for the largest value of Γ the period is monotonic as a function of $\check{c}$. Detailed numerical investigation shows that the local maxima of the period as a function of $\check{c}$ trace out a locus in the Γ–$\check{c}$ plane that is illustrated in Figure 2.1. The "ridge" in the period intersects the Hopf bifurcation locus at $\Gamma = 0.345$ (see Figure 2.1). Note that the limiting period on the Hopf bifurcation locus is $\sqrt{1 - \check{c}\,\Gamma_H(\check{c})}$, which is an increasing function of $\check{c}$.

For the full Klausmeier model (1.1), contours of constant wavelength also show a ridge close to the Hopf bifurcation locus, above the Turing bifurcation point (see

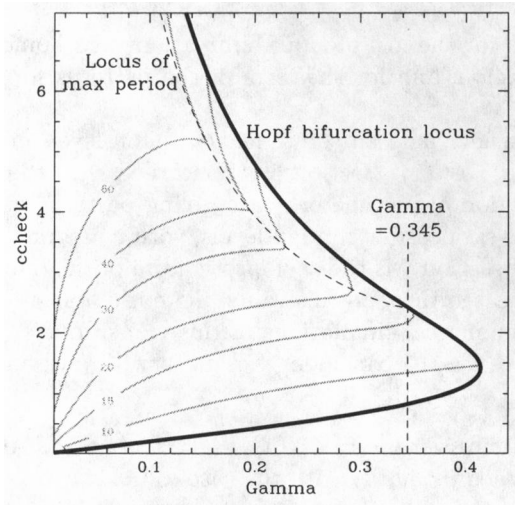

FIG. 2.1. *Existence of periodic solutions of* (2.1). *The thick black line shows the locus of Hopf bifurcation points of* $(\check{U}, \check{W}) = (1, 1)$ *in the* Γ–$\check{c}$ *plane; periodic solutions exist to the left of this curve. The grey lines show contours of constant period. The dashed curve shows the locus of local maxima of the period as a function of* $\check{c}$. *The vertical dashed line indicates the value of* Γ *at which this locus of maxima intersects the Hopf bifurcation locus. The calculation of the Hopf bifurcation locus and the period contours, and also the plotting, were done using the software package* WAVETRAIN [35, 36]. *The maximum period locus was calculated from solution branches such as those illustrated in Figure* 2.2, *via quadratic interpolation. Full details of the* WAVETRAIN *input files, run commands (including run times), and plot commands are given at* http://www.ma.hw.ac.uk/~jas/supplements/kl5.

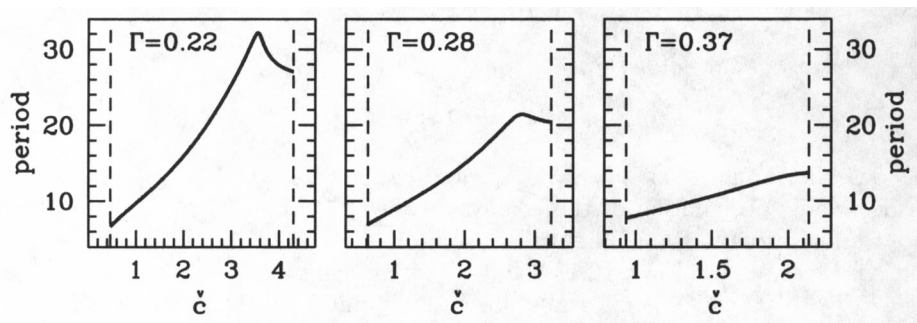

FIG. 2.2. *Plots of periodic solution branches of* (2.1). *I plot the period as a function of the rescaled speed* $\check{c}$ *for three different values of the parameter* Γ. *The vertical dashed lines denote the Hopf bifurcation points, which are the end points of the solution branches. For* $\Gamma = 0.22$ *and* $\Gamma = 0.28$ *there is a local maximum in the period at a point between the Hopf bifurcation values, whereas for* $\Gamma = 0.37$ *the period is monotonic as a function of* $\check{c}$. *The transition to monotonicity occurs at* $\Gamma = 0.345$ *(see Figure* 2.1*). The solutions were calculated using the numerical continuation package* AUTO [39, 40, 41].

Figure 1.2). My results show that as ν is increased so that the Turing bifurcation point of (1.1) moves further to the right in the A–c plane, this ridge remains localized near the Hopf bifurcation locus, with $A = O_s(\nu^{1/2})$ on both curves.

3. Pattern solutions for $c = O_s(1)$, $\nu^{-1/2} \ll A \ll \nu^{1/2}$. Close to the Hopf bifurcation locus in the A–c plane, the patterns consist of relatively gentle oscillations. However, as A is gradually decreased with fixed c, the solution profile develops an increasingly spiked appearance. The separation of the spikes is proportional to $\nu^{1/2}/A$,

while their separation is $O_s(1)$ as $\nu \to \infty$. Therefore for $A \ll \nu^{1/2}$ the patterns must be studied via two matched layers. In this section I will derive the leading order form of this matched asymptotic solution.

Between the spikes, I write $U = A^{1/2}\nu^{1/4}c^{1/2}U_{\text{inter}}$, $W = \nu^{-1/2}W_{\text{inter}}$, and $z = (\nu^{1/2}/A)z_{\text{inter}}$. Note that the factor of $A^{1/2}$ in the scaling of U includes some ν-dependence; the factor of $c^{1/2}$ is also included because it gives simpler algebra when matching to the spike solution. Substituting these rescalings into (1.2) gives, to leading order as $\nu \to \infty$, $U_{\text{inter}} = 0$ and $dW_{\text{inter}}/dz_{\text{inter}} + 1 = 0 \Rightarrow W_{\text{inter}} = k_{\text{inter}} - z_{\text{inter}}$, where k_{inter} is a constant of integration. Note that in fact all terms of algebraic order in the asymptotic expansion for U_{inter} are identically zero.

For the spikes, I again use c as well as ν in the rescalings for algebraic convenience: $U = \nu^{1/2}c^{1/2}U_{\text{spike}}$, $W = \nu^{-1/2}c^{3/2}W_{\text{spike}}$, and $z = c^{-1}z_{\text{spike}}$. These imply

$$dU_{\text{spike}}/dz_{\text{spike}} = V_{\text{spike}}, \tag{3.1a}$$

$$dV_{\text{spike}}/dz_{\text{spike}} = -V_{\text{spike}} - W_{\text{spike}}U_{\text{spike}}^2 + (B/c^2)U_{\text{spike}}, \tag{3.1b}$$

$$dW_{\text{spike}}/dz_{\text{spike}} = W_{\text{spike}}U_{\text{spike}}^2, \tag{3.1c}$$

to leading order as $\nu \to \infty$. I have been unable to solve (3.1) exactly, but some insight is given by integrating across the spike. Eliminating the $W_{\text{spike}}U_{\text{spike}}^2$ term between the equations and integrating between $z_{\text{spike}} = -\infty$ and $z_{\text{spike}} = +\infty$ gives

$$[W_{\text{spike}}]_{-\infty}^{+\infty} = (B/c^2)\int_{-\infty}^{+\infty} U_{\text{spike}}\, dz_{\text{spike}}.$$

Simple matching of the spike and interspike regions requires $c^{3/2}W_{\text{spike}}(z_{\text{spike}} = -\infty) = k_{\text{inter}} - z_{\text{inter}}^{**}$ and $c^{3/2}W_{\text{spike}}(z_{\text{spike}} = +\infty) = k_{\text{inter}} - z_{\text{inter}}^{*}$, where $z_{\text{inter}} = z_{\text{inter}}^{*}$ and $z_{\text{inter}} = z_{\text{inter}}^{**}$ are the locations of consecutive spikes ($z_{\text{inter}}^{**} > z_{\text{inter}}^{*}$). Therefore the pattern wavelength L is given by

$$L = \frac{\nu^{1/2}}{A}\left(z_{\text{inter}}^{**} - z_{\text{inter}}^{*}\right) = \frac{\nu^{1/2}c^{3/2}}{A}\left[W_{\text{spike}}\right]_{-\infty}^{+\infty} = \frac{\nu^{1/2}B}{c^{1/2}A}\int_{-\infty}^{+\infty} U_{\text{spike}}\, dz_{\text{spike}}. \tag{3.2}$$

In (3.1), the W_{spike}-axis ($U_{\text{spike}} = V_{\text{spike}} = 0$) is a line of equilibria. Straightforward calculation shows that there are two real eigenvalues at each point on this line, one positive and one negative, with the corresponding eigenvectors being orthogonal to the W_{spike}-axis. The third eigenvalue is zero and corresponds to the neutral stability along the W_{spike}-axis.

Numerical calculation of trajectories leaving the W_{spike}-axis along the unstable eigenvector suggests that they all go to infinity with a single exception; for this unique starting value of W_{spike}, the trajectory terminates back on the W_{spike}-axis, giving a heteroclinic connection that corresponds to the spike. The start- and end values of W_{spike} for this connection can be determined via numerical shooting, and Figure 3.1(a) illustrates the two values of W_{spike} as a function of B/c^2, which is the only parameter grouping in (3.1). The difference between these values of W_{spike} then gives the pattern wavelength using (3.2), and the dependence of this on the migration speed c is illustrated in Figure 3.1(b). The increase in wavelength with c is consistent with the result from section 2 that the ridge in the pattern wavelength in the A–c plane is restricted to values of A that are $O_s(\nu^{1/2})$.

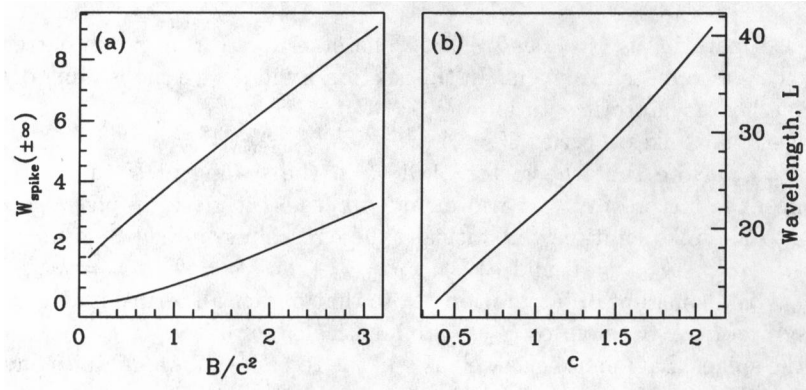

FIG. 3.1. (a) *Numerical calculations of the start- and end values of* W_{spike} *for the heteroclinic connection in* (3.1), *which corresponds to the spike in vegetation density for* $\nu^{-1/2} \ll A \ll \nu^{1/2}$. *The two values are plotted as a function of* B/c^2, *which is the only parameter grouping in* (3.1). *I calculated* $W_{\text{spike}}(\pm\infty)$ *using a shooting method, which is described in Appendix* A. *Note that* $W_{\text{spike}}(-\infty) < W_{\text{spike}}(+\infty)$, *from* (3.1). (b) *The dependence of the wavelength* L *on migration speed* c *when* $\nu^{-1/2} \ll A \ll \nu^{1/2}$. L *is determined by* $W_{\text{spike}}(\pm\infty)$ *via* (3.2), *and the numerical values shown are for* $A = 1.5$, $B = 0.45$, $\nu = 182.5$.

4. Pattern solutions for $c = O_s(1)$, $A = O_s(\nu^{-1/2})$. In this section I extend the work in section 3 to $A = O_s(1)$. My key result is the leading order form of the homoclinic locus that forms the left-hand boundary of the parameter regions giving patterns in the A–c plane. One implication of this is a leading order formula for the value of the rainfall parameter A at the fold in the homoclinic locus; this is the minimum possible rainfall level at which vegetation can survive.

The solutions derived in section 3 are valid only when $\nu^{-1/2} \ll A \ll \nu^{1/2}$. For $A = O_s(\nu^{1/2})$, the scalings used for z within and between the spikes become the same, so that the solution loses its two-layered structure: this was the case discussed in section 2. However, for $A = O_s(\nu^{-1/2})$ there is no change in the solution structure, which again consists of sharp spikes whose separation is $\gg 1$ as $\nu \to \infty$. The scalings used in section 3 remain valid, as does the leading order spike solution derived in section 3. Also $U_{\text{inter}} \equiv 0$, as in section 3. The difference when $A = O_s(\nu^{1/2})$ comes in the leading order equation for the water density W between the spikes, which contains an additional term: $dW_{\text{inter}}/dz_{\text{inter}} + 1 - W_{\text{inter}}/(A\nu^{1/2}) \Rightarrow W_{\text{inter}} = A\nu^{1/2} - \bar{k}_{\text{inter}} \exp(z_{\text{inter}}/A\nu^{1/2})$, where $\bar{k}_{\text{inter}}$ is a constant of integration.

Matching of the spike and interspike regions now requires $c^{3/2}W_{\text{spike}}(z_{\text{spike}} = -\infty) = A\nu^{1/2} - \bar{k}_{\text{inter}} \exp(z^{**}_{\text{inter}}/A\nu^{1/2})$ and $c^{3/2}W_{\text{spike}}(z_{\text{spike}} = +\infty) = A\nu^{1/2} - \bar{k}_{\text{inter}} \exp(z^{*}_{\text{inter}}/A\nu^{1/2})$; as in section 3, $z_{\text{inter}} = z^{*}_{\text{inter}}$ and $z_{\text{inter}} = z^{**}_{\text{inter}}$ are the locations of consecutive spikes ($z^{**}_{\text{inter}} > z^{*}_{\text{inter}}$). Therefore the pattern wavelength L is given by

$$L = \frac{\nu^{1/2}}{A}\left(z^{**}_{\text{inter}} - z^{*}_{\text{inter}}\right) = \nu \log\left[\frac{A\nu^{1/2} - c^{3/2}W_{\text{spike}}(-\infty)}{A\nu^{1/2} - c^{3/2}W_{\text{spike}}(+\infty)}\right]. \tag{4.1}$$

Since $W_{\text{spike}}(+\infty) > W_{\text{spike}}(-\infty)$, the expression in (4.1) is finite and positive, provided that $A > \nu^{-1/2}c^{3/2}W_{\text{spike}}(+\infty) \equiv A_{hc}$, with the wavelength tending to infinity as A approaches this lower limit. Therefore $A = A_{hc}$ is the leading order form of the homoclinic locus that forms the left-hand boundary of the parameter region giving patterns in Figure 1.2. Between the spikes, $U_{\text{inter}} = 0$ with W_{inter} decaying to $A\nu^{1/2}$ to leading order, which corresponds to the "desert" steady state $(u, w) = (0, A)$ of

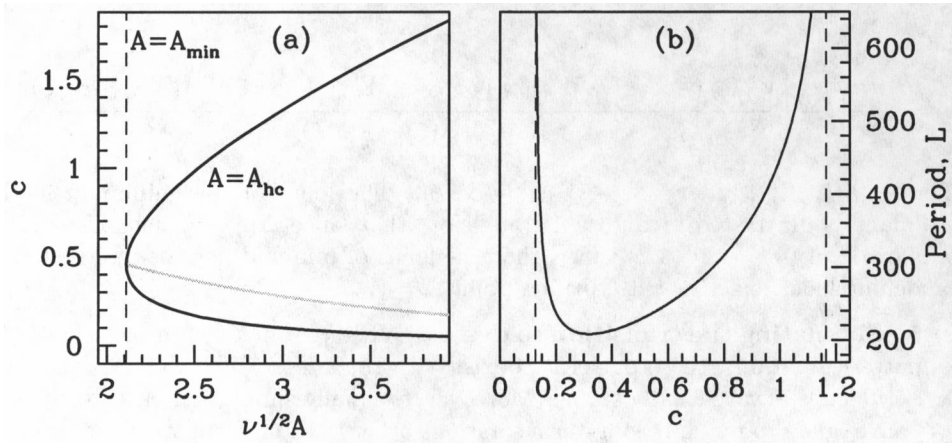

FIG. 4.1. (a) *An illustration of A_{hc} as a function of the migration speed c (black curve) for $B = 0.45$. This is the leading order form (as $\nu \to \infty$) of the locus of homoclinic solutions when $A = O_s(\nu^{-1/2})$. The locus was calculated using* (4.2)*, with $W_{\text{spike}}(+\infty)$ calculated using the algorithm described in Appendix* A*. The vertical dashed line shows A_{min}, the leading order form of the minimum rainfall level at which banded vegetation is possible. I have superimposed on this plot the locus (grey curve) of the migration speed giving the minimum wavelength for a given value of A. This is evaluated using the formula* (4.3)*, with $W_{\text{spike}}(\pm\infty;\xi)$ and $(d/d\xi)W_{\text{spike}}(\pm\infty;\xi)$ calculated using the algorithm described in Appendix* A*. Note that this locus of minima intersects the locus of homoclinic solutions at $A = A_{min}$.* (b) *A typical example of the variation in pattern wavelength L with migration speed c, to leading order as $\nu \to \infty$ with $A = O_s(\nu^{-1/2})$ fixed. The case shown is for $A = 2.75$, $B = 0.45$, $\nu = 182.5$. L is given by the formula* (4.1)*, and I evaluated $W_{\text{spike}}(\pm\infty)$ numerically using the algorithm described in Appendix* A*. The vertical dashed lines show the values of c giving homoclinic solutions, to leading order as $\nu \to \infty$.*

(1.1). Therefore the homoclinic solution is homoclinic to this desert steady state.

Using my numerical algorithm for $W_{\text{spike}}(+\infty)$ (described in Appendix A), it is straightforward to calculate A_{hc}, and its dependence on c is illustrated in Figure 4.1(a). A key feature of this figure is the turning point, at $A = A_{min}$. This is the lowest rainfall level at which patterns can be sustained: below this, only full-blown desert is possible. To investigate this critical value of A in more detail, it is convenient to replace c by $\xi = B/c^2$ $(\xi > 0)$; recall that equations (3.1) depend only on this single parameter grouping. Then

$$A_{hc} = \nu^{-1/2} B^{3/4} \xi^{-3/4} W_{\text{spike}}(+\infty;\xi), \tag{4.2}$$

and A_{min} corresponds to $(d/d\xi)\left[\xi^{-3/4}W_{\text{spike}}(+\infty;\xi)\right] = 0$; i.e., $3W_{\text{spike}}(+\infty;\xi) = 4\xi\frac{d}{d\xi}W_{\text{spike}}(+\infty;\xi)$. In Appendix A, I describe a numerical algorithm for the calculation of $(d/d\xi)W_{\text{spike}}(+\infty;\xi)$, which gives the solution of this equation as $\xi = 2.1654$, implying $A_{min} = 3.8405B^{3/4}\nu^{-1/2}$.

In [34, section 5.2] I showed that for $1/\nu \ll c \ll 1$ as $\nu \to \infty$, the leading order form of the homoclinic locus is $A = (24/7)^{1/2}Bc^{-1/2}\nu^{-1/2}$. Formula (4.2) is consistent with that result if and only if $W_{\text{spike}}(+\infty;\xi) \sim (24/7)^{1/2}\xi$ as $\xi \to \infty$, and this is confirmed by numerical calculations.

For $A > A_{hc}$, but still with $A = O_s(\nu^{1/2})$, numerical evaluation of (4.1) indicates that the wavelength L is a unimodal function of c, with a single local minimum, and with the period increasing to infinity at the homoclinic points on either side. A typical example is illustrated in Figure 4.1(b). Differentiating (4.1) with respect to ξ shows that the minimum period occurs at

(4.3)
$$A = \frac{B^{3/4}\xi^{1/4}}{\nu^{1/2}}\left[\frac{W_{\text{spike}}(-\infty;\xi)\,\frac{d}{d\xi}W_{\text{spike}}(+\infty;\xi) - W_{\text{spike}}(+\infty;\xi)\,\frac{d}{d\xi}W_{\text{spike}}(-\infty;\xi)}{\xi\,\frac{d}{d\xi}\Delta(\xi) - \frac{3}{4}\Delta(\xi)}\right],$$

where $\Delta(\xi) = W_{\text{spike}}(+\infty;\xi) - W_{\text{spike}}(-\infty;\xi)$. The locus of this minimum in the A–c plane is illustrated in Figure 4.1(a). Note that since $\Delta(\xi) \to 0$ as $A \to A^{+}_{min}$, comparison of (4.3) and (4.2) shows that the locus of minimal periods intersects the homoclinic locus exactly at its turning point $A = A_{min}$.

5. Simulating the transition to desert. When parameters are such that (1.1) has pattern solutions, these patterns coexist with the "desert" steady state $(u, w) = (0, A)$, which is always locally stable. Moreover, the many simulation-based studies of (1.1) have failed to find any long-term solutions other than uniform steady states and constant speed periodic patterns (e.g., [14, 20, 42]). Therefore the minimum rainfall level giving patterns is of major ecological significance, representing a threshold below which no vegetation can be sustained, so that full-blown desert is inevitable. In his original paper, Klausmeier [14] speculated that this threshold was $2B$, which is the minimum rainfall level for the existence of a homogeneous vegetated steady state. However, Klausmeier overlooked the fact that in a nonlinear model, pattern solution branches that emanate from a Hopf bifurcation of a steady state can extend to parameter values for which that steady state does not exist. This is indeed the case for the model (1.1), and numerical work has shown that the minimum rainfall level for patterns is significantly below $2B$ [43]. From an ecological viewpoint the explanation for this is that patterned vegetation can exist at rainfall levels that are too low for homogeneous vegetation. Here, for the first time, I have derived the asymptotic form of the threshold for large ν, namely, $A_{min} = 3.8405B^{3/4}\nu^{-1/2}$.

To emphasize the significance of this threshold value of the rainfall parameter, I undertook a numerical study of the transition to desert, as predicted by (1.1). My results are illustrated in Figure 5.1. With the values of B and ν as in Figure 1.2, I began by calculating the pattern solution for $A = 0.6$ with wavelength 100; this

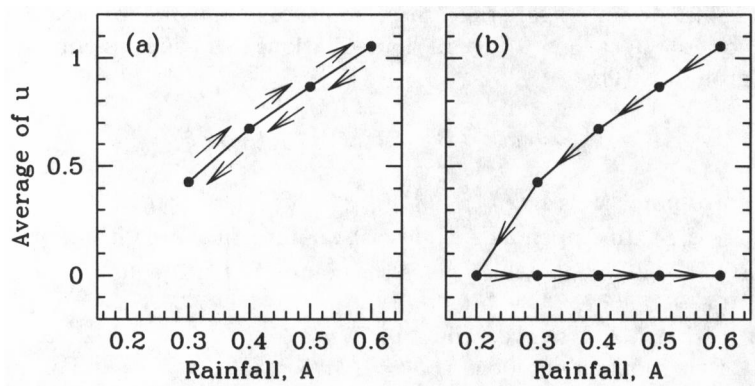

FIG. 5.1. *An illustration of a permanent transition to total desert in the Klausmeier model* (1.1). *With A initially set to* 0.6, *I solved* (1.1) *numerically as described in the legend to Figure* 1.1, *changing the rainfall parameter by* 0.1 *every* 1000 *time units. The initial conditions were the pattern solution for* $A = 0.6$ *with wavelength* 100, *which has* $c = 1.499$. *I plot A against the mean value of the vegetation density u.* (a) *shows the results when A is decreased to* 0.3 *and then increased back to* 0.6: *the mean vegetation density decreases with A and then follows a reverse trend when A is increased again.* (b) *shows that when A is decreased further to* 0.2, *vegetation is lost, and the solution then remains in this "desert state" when A is increased again.*

uniquely determines $c = 1.499$. I then used this as an initial condition for the numerical solution of (1.1) on a domain of length 100, with periodic boundary conditions. I gradually decreased A in steps of 0.1, solving (1.1) for a time interval of 1000 at each value of A. As A is decreased down to 0.3, the solution continues to have the form of a single spike in vegetation density. If A is now increased again in steps of 0.1, the progress of the solution is simply reversed (Figure 5.1(a)). However, further decrease in A to 0.2 causes the patterned (vegetated) state to be lost, and instead the solution approaches the desert steady state (Figure 5.1(b)). A subsequent increasing of A does not reverse the behavior; rather, the solution remains at this desert steady state.

The critical level of the rainfall parameter A, between 0.2 and 0.3, at which vegetation is lost in this simulation is greater than $3.8405B^{3/4}\nu^{-1/2} \approx 0.16$. This is because the patterns that exist for A between 0.16 and 0.2 have wavelengths greater than 100 and are therefore incompatible with the boundary conditions used in the simulation. In the field, vegetation patterns typically occur in regions of very large spatial extent, so that $3.8405B^{3/4}\nu^{-1/2}$ is the relevant threshold. A key prediction of the Klausmeier model (1.1) is that a decrease in the rainfall level below this threshold heralds the onset of desertification, and moreover the loss of vegetation is permanent, in the sense that it cannot be reinstated by simply increasing rainfall levels. Similar behavior has been found previously in other models of banded vegetation [16, 21]. Consequently the rainfall threshold that I have calculated is of considerable potential value for the management of ecosystems containing banded vegetation.

6. Pattern solutions for $1 \ll c \ll \nu^{1/2}$. In sections 3 and 4, I studied the existence and form of pattern solutions of (1.1) when $c = O_s(1)$ as $\nu \to \infty$. I now extend this to the case of $1 \ll c \ll \nu^{1/2}$. I will derive leading order formulae for the boundaries of the parameter region giving patterns, and I will show that there is an abrupt change in pattern form as parameters are varied, at a point whose leading order location I will derive. Note that beyond the scaling range considered in this section, at $c = O_s(\nu^{1/2})$ the solution structure changes completely: there is an intersection of two different loci of homoclinic solutions, which can be seen at $(A, c) \approx (1.6, 6.6)$ in Figure 1.2(a). Details of this intersection and of pattern solutions when $c = O_s(\nu^{1/2})$ are given in [33].

For $c = O_s(1)$ patterns exist between a locus of Hopf bifurcations and a locus of homoclinic solutions in (1.2), and this also applies for $1 \ll c \ll \nu^{1/2}$. Again, as for $c = O_s(1)$, different solution structures apply in the vicinity of the Hopf bifurcation locus and in the remainder of parameter space, and I consider the latter case first. In sections 3 and 4, I showed that for $c = O_s(1)$ patterns away from the Hopf bifurcation locus are composed of a spike layer and an interspike region. Valuable insight into the corresponding structure for $1 \ll c \ll \nu^{1/2}$ is given by the change in the form of the spike solutions $(U_{\text{spike}}, W_{\text{spike}})$ of (3.1) as a function of z_{spike} as c increases (Figure 6.1). The front of the spike remains of approximately constant width, while the back becomes progressively wider as c increases. The culmination of this behavior is that for $1 \ll c \ll \nu^{1/2}$ the spike solution separates into two sublayers, with different scalings for z:

(6.1)

$$\text{Spike layer 1:} \quad U = \nu^{1/2}c^{1/2}\widehat{U}_{\text{spike1}}, \quad W = \nu^{-1/2}c^{3/2}\widehat{W}_{\text{spike1}}, \quad z = c\,\hat{z}_{\text{spike1}},$$

(6.2)

$$\text{Spike layer 2:} \quad U = \nu^{1/2}c^{1/2}\widehat{U}_{\text{spike2}}, \quad W = \nu^{-1/2}c^{3/2}\widehat{W}_{\text{spike2}}, \quad z = c^{-1}\hat{z}_{\text{spike2}}.$$

Here I use hats to distinguish the present case from those discussed in sections 3 and 4. I will show that these scalings are relevant when $c^{3/2}/\nu^{1/2} = O(A)$ and

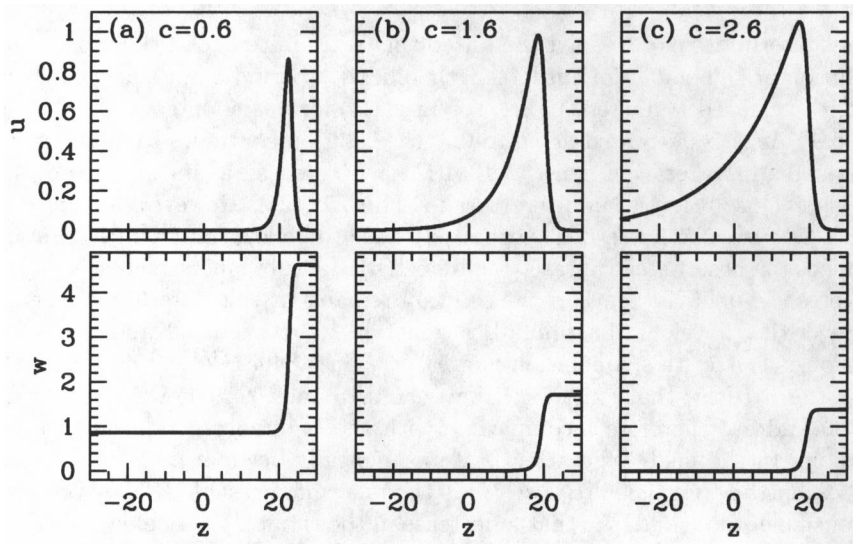

FIG. 6.1. *The variation with c of the spike solution discussed in section 3. I plot the solution of* (3.1) *that begins and ends on the* $U_{\text{spike}} = V_{\text{spike}} = 0$ *axis for three different values of* $\xi = B/c^2$*; the values of c shown in the figure are for* $B = 0.45$*. The figure shows that the width of the front of the spike is approximately independent of c, while the back becomes wider as c increases.*

$A = O(\nu^{1/2}/c^{1/2})$; the homoclinic locus occurs when $A = O_s(c^{3/2}/\nu^{1/2})$, while $A = O_s(\nu^{1/2}/c^{1/2})$ gives the Hopf bifurcation locus.

Solution in spike layer 1. For $c^{3/2}/\nu^{1/2} = O(A)$ and $A = O(\nu^{1/2}/c^{1/2})$, substituting (6.1) into (1.2a) gives $\widehat{W}_{\text{spike1}}\widehat{U}^2_{\text{spike1}} = o(1)$ as $\nu \to \infty$. If $\widehat{U}_{\text{spike1}} = o(1)$, then (1.2b) implies that $\widehat{W}_{\text{spike1}}$ is a constant, which cannot match with the other solution layers (details omitted for brevity). Therefore $\widehat{W}_{\text{spike1}} = o(1)$. The same argument shows that the smallest nonzero term in the asymptotic expansion for $\widehat{W}_{\text{spike1}}$ must satisfy $\widehat{W}_{\text{spike1}}\widehat{U}^2_{\text{spike1}} = O_s(Ac^{-5/2}\nu^{-1/2})$. Therefore the $\widehat{W}_{\text{spike1}}\widehat{U}^2_{\text{spike1}}$ term is negligible in (1.2a), which implies the leading order solution $\widehat{U}_{\text{spike1}} = \widehat{K}_{\text{spike1}}e^{B\hat{z}_{\text{spike1}}}$, where $\widehat{K}_{\text{spike1}}$ is a constant of integration.

Solution in spike layer 2. Substituting (6.2) into (1.2) gives leading order equations which can be integrated once, yielding

$$d\widehat{U}_{\text{spike2}}/d\hat{z}_{\text{spike2}} = -\widehat{U}_{\text{spike2}} - \widehat{W}_{\text{spike2}} + \widehat{K}_{\text{spike2}}, \tag{6.3a}$$

$$d\widehat{W}_{\text{spike2}}/d\hat{z}_{\text{spike2}} = \widehat{U}^2_{\text{spike2}}\widehat{W}_{\text{spike2}}, \tag{6.3b}$$

where $\widehat{K}_{\text{spike2}}$ is a constant of integration. Equations (6.3) also feature in the solution of (1.1) when $c = O_s(\nu^{1/2})$, and in [33, Proposition 3] I proved that there is a bifurcation at $\widehat{K}_{\text{spike2}} = \widehat{K}^*_{\text{spike2}} \approx 1.1606$. For $\widehat{K}_{\text{spike2}} \le \widehat{K}^*_{\text{spike2}}$ there is exactly one trajectory connecting the two steady states $(\widehat{K}_{\text{spike2}}, 0)$ and $(0, \widehat{K}_{\text{spike2}})$; its departure from $(0, \widehat{K}_{\text{spike2}})$ is algebraic in $\hat{z}_{\text{spike2}}$ if $\widehat{K}_{\text{spike2}} < \widehat{K}^*_{\text{spike2}}$, and exponential if $\widehat{K}_{\text{spike2}} = \widehat{K}^*_{\text{spike2}}$. For $\widehat{K}_{\text{spike2}} > \widehat{K}^*_{\text{spike2}}$ there are no trajectories connecting the two steady states.

Solution between the spikes. The appropriate rescalings between the spikes are $U = \nu^{1/2}c^{1/2}\widehat{U}_{\text{inter}}$, $W = \nu^{-1/2}c^{3/2}\widehat{W}_{\text{inter}}$, and $z = c^{3/2}\nu^{1/2}A^{-1}\hat{z}_{\text{inter}}$. As in sections 3

and 4, substitution of these rescalings into (1.2) implies that $\widehat{U}_{\text{inter}} \equiv 0$, with

(6.4)
$$\widehat{W}_{\text{inter}} = \begin{cases} \widehat{K}_{\text{inter},1} - \hat{z}_{\text{inter}} & \text{if } c^{3/2}/\nu^{1/2} = O(A) \text{ and } A = O(\nu^{1/2}/c^{1/2}), \\ A\nu^{1/2}c^{-3/2} - \widehat{K}_{\text{inter},2} \exp\{\hat{z}_{\text{inter}} c^{3/2} A^{-1} \nu^{-1/2}\} & \text{if } A = O_s(c^{3/2}/\nu^{1/2}), \end{cases}$$

to leading order as $\nu \to \infty$, where $\widehat{K}_{\text{inter},1}$ and $\widehat{K}_{\text{inter},2}$ are constants of integration.

Matching the three layers. Matching between the two spike layers requires that $\lim_{\hat{z}_{\text{spike2}} \to \infty} (\widehat{U}_{\text{spike2}}, \widehat{W}_{\text{spike2}})$ be equal to $(\widehat{U}_{\text{spike1}}, \widehat{W}_{\text{spike1}})$ at an arbitrary finite value of $\hat{z}_{\text{spike1}}$, which I take to be zero. Therefore $\widehat{U}_{\text{spike2}}(\infty) = \widehat{K}_{\text{spike1}}$ and $\widehat{W}_{\text{spike2}}(\infty) = 0$. I denote by $\hat{z}_{\text{inter}} = \hat{z}^*_{\text{inter}}$ and $\hat{z}^{**}_{\text{inter}}$ the locations of two consecutive spikes ($\hat{z}^{**}_{\text{inter}} > \hat{z}^*_{\text{inter}}$). Then matching between spike layer 1 and the interspike solution (6.4) requires $\widehat{U}_{\text{spike2}}(-\infty) = 0$ and $\widehat{W}_{\text{spike2}}(-\infty) = \widehat{W}_{\text{inter}}(\hat{z}^*_{\text{inter}})$. This finite start point for the solution trajectory of (6.3) must be the steady state $(0, \widehat{K}_{\text{spike2}})$. Therefore $(\widehat{U}_{\text{spike2}}, \widehat{W}_{\text{spike2}})$ must connect the two steady states of (6.3). Moreover, the behavior near $(0, \widehat{K}_{\text{spike2}})$ must be exponential in $\hat{z}_{\text{spike2}}$; otherwise there would be algebraic terms needing to be matched at higher order, which contradicts $\widehat{U}_{\text{inter}} \equiv 0$. As discussed above, this specifies the solution and uniquely determines $\widehat{K}_{\text{spike2}} = \widehat{K}^*_{\text{spike2}}$. Finally, matching the interspike solution and spike layer 1 requires $\widehat{W}_{\text{inter}}(\hat{z}^{**}_{\text{inter}}) = 0$. Combining these various matching conditions gives $\widehat{K}_{\text{spike1}} = \widehat{K}^*_{\text{spike2}}$, and also

$$\begin{aligned} c^{3/2}/\nu^{1/2} = O(A) \text{ and } A = O(\nu^{1/2}/c^{1/2}): \quad & \widehat{K}_{\text{inter},1} - \hat{z}^*_{\text{inter}} = \widehat{K}^*_{\text{spike2}} \\ & \text{and} \quad \widehat{K}_{\text{inter},1} - \hat{z}^{**}_{\text{inter}} = 0 \\ & \Rightarrow \quad L = \widehat{K}^*_{\text{spike2}} c^{3/2} \nu^{1/2} / A, \end{aligned} \tag{6.5}$$

$$\begin{aligned} A = O_s(c^{3/2}/\nu^{1/2}): \quad & A\nu^{1/2}c^{-3/2} - \widehat{K}_{\text{inter},2} \exp\{\hat{z}^*_{\text{inter}} c^{3/2} A^{-1} \nu^{-1/2}\} = \widehat{K}^*_{\text{spike2}} \\ \text{and} \quad & A\nu^{1/2}c^{-3/2} - \widehat{K}_{\text{inter},2} \exp\{\hat{z}^{**}_{\text{inter}} c^{3/2} A^{-1} \nu^{-1/2}\} = 0 \\ \Rightarrow \quad & L = \nu \log\left[\nu^{1/2} A / \left(\nu^{1/2} A - \widehat{K}^*_{\text{spike2}} c^{3/2}\right)\right], \end{aligned} \tag{6.6}$$

where $L = (\hat{z}^{**}_{\text{inter}} - \hat{z}^*_{\text{inter}}) c^{3/2} \nu^{1/2} A^{-1}$ is the leading order pattern wavelength. Note that L is independent of B to leading order in both cases. This is an interesting result from the viewpoint of land management. Numerical simulations of (1.1) show that slow changes in parameters cause the migration speed of the observed patterns to change in order to preserve the pattern wavelength [43, 44]. Hence in this parameter regime, changes in grazing intensity will not affect either the migration speed of patterns or their wavelength—though of course it will affect the vegetation density in the bands.

This completes the calculation of the leading order form of the pattern solution for $c^{3/2}/\nu^{1/2} = O(A)$, $A = O(\nu^{1/2}/c^{1/2})$. Its key implication comes from (6.6): $L \to \infty$ as $A \to \widehat{A}^+_{hc}$, where $\widehat{A}_{hc} = c^{3/2}\widehat{K}^*_{\text{spike2}}/\nu^{1/2}$; recall that $\widehat{K}^*_{\text{spike2}} \approx 1.1606$. Hence the leading order form of the left-hand boundary of the parameter region giving patterns in the A–c plane is the homoclinic locus $A = \widehat{A}_{hc}$. Consistency between this result and (4.2) requires that $W_{\text{spike}}(+\infty; \xi) \to \widehat{K}^*_{\text{spike2}}$ as $\xi \to 0^+$, and this is confirmed by numerical calculations.[1] My expression for $\widehat{A}_{hc}$ is also consistent with

[1] Note that $W_{\text{spike}}(\cdot\,; \xi)$ is defined only for $\xi > 0$. Equations (3.1) are of course well defined at $\xi = 0$, but the limit is a singular one (see Figure 6.1 and the associated discussion).

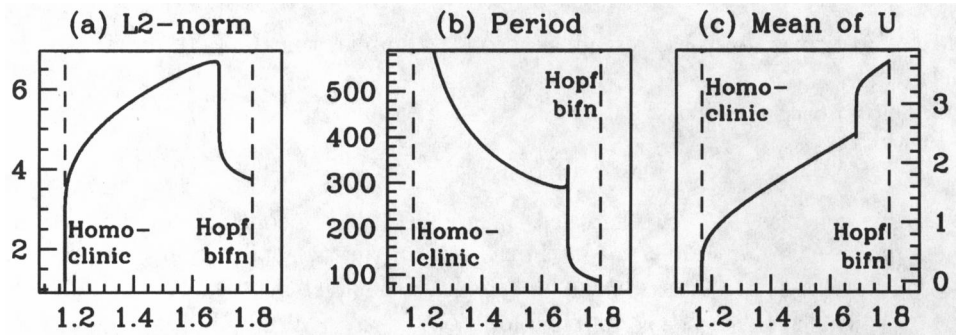

FIG. 6.2. *An illustration of the abrupt change in pattern form that occurs as the rainfall A is varied, when* $1 \ll c \ll \nu^{1/2}$ *as* $\nu \to \infty$. *I plot three solution measures as a function of A for* $B = 0.45$ *and* $\nu = 182.5$: *the* L_2 *norm of the solution of* (1.2), *the period, and the mean value of U over one period. The vertical dashed lines indicate the values of A at the Hopf bifurcation point and the homoclinic solution; these are the end points of the solution branch. The results were obtained by numerical continuation of the limit cycle branch of* (1.2) *starting from the Hopf bifurcation point, using the software package* AUTO [39, 40, 41].

the leading order form of the homoclinic locus when $c = O_s(\nu^{1/2})$, which is derived in [33, section 4.4].

The scaling $A = O_s(\nu^{1/2}/c^{1/2})$ includes the Hopf bifurcation locus, and patterns in the vicinity of this locus have relatively gentle oscillations, in contrast to the spiked solutions discussed above. To study patterns in this parameter regime, I follow [31, 33] and use the scalings for U, W, and z corresponding to the steady state (u_s, w_s) and the limiting period of the limit cycles at the Hopf bifurcation point, namely, $\tilde{U} = (B/A)U$, $\tilde{W} = (A/B^2)W$, and $\tilde{z} = (B/c)z$. Substituting these into (1.2) gives

$$d\tilde{U}/d\tilde{z} = \tilde{U} - \tilde{U}^2\tilde{W}, \tag{6.7a}$$

$$d\tilde{W}/d\tilde{z} = \sigma^2(\tilde{U}^2\tilde{W} - 1), \tag{6.7b}$$

to leading order as $\nu \to \infty$; here $\sigma = Ac^{1/2}/\nu^{1/2}B^{3/2}$, which is $O_s(1)$. Equations (6.7) also arise for $c \gg \nu^{1/2}$, and I have studied them in detail in [31]. The key result is that the unique steady state $(\tilde{U}, \tilde{W}) = (1, 1)$ undergoes a subcritical Hopf bifurcation at $\sigma = 1$, while at $\sigma = \sigma^* \approx 0.9003$ there is a homoclinic solution that is homoclinic to a point at infinity. Numerical continuation suggests that the branch of limit cycles varies monotonically in σ between these end points.

For $c = O_s(1)$ as $\nu \to \infty$, I showed in sections 3 and 4 that there is a gradual transition from the gentle oscillations that occur in the vicinity of the Hopf bifurcation locus to the spiked patterns that occur for smaller values of A. For $1 \ll c \ll \nu^{1/2}$ the patterns close to the Hopf bifurcation locus are given by the limit cycles of (6.7), to leading order as $\nu \to \infty$. However, these exist only for $A > \sigma^*\nu^{1/2}B^{3/2}/c^{1/2}$. This suggests a more abrupt change in pattern form, which is confirmed by numerical continuation of the solutions of (1.2). Figures 6.2(a) and (b) illustrate switching in the norm and period of patterns as A is varied for a fixed value of c. The key to understanding this switching is the fact that the homoclinic solution of (6.7) that occurs at $\sigma = \sigma^*$ is homoclinic to a point at infinity. As σ approaches σ^* from above, the maxima $\tilde{U}_{max}$ and $\tilde{W}_{max}$ of $\tilde{U}$ and $\tilde{W}$ tend to infinity. Therefore for A sufficiently close to $\sigma^*\nu^{1/2}B^{3/2}/c^{1/2}$, (6.7) is no longer the leading order form of (1.2) as $\nu \to \infty$: for instance, the term W $(= (B^2/A)\tilde{W})$ in (1.2b) will become comparable in size to A. Therefore the structure of pattern solutions changes over an A-interval adjacent to

$\sigma^* \nu^{1/2} B^{3/2}/c^{1/2}$ whose width is $o(1)$ as $\nu \to \infty$. In fact, numerical solutions of (6.7) suggest that $\tilde{U}_{max}$, $\tilde{W}_{max} = O_s\big(\log(\sigma - \sigma^*)\big)$ as $\sigma \to \sigma^{*+}$ [31, Figure 5], implying that the width of this transition interval is exponentially small in ν as $\nu \to \infty$. I have not investigated the details of the solution in this transition interval, and this is a natural area for future work.

From the viewpoint of land management, the abrupt change in pattern form as rainfall varies is very significant. Figure 6.2(c) shows that it implies a sharp drop in mean vegetation density as rainfall is gradually decreased. Many semiarid regions with banded vegetation are used for grazing and/or timber [45, 46]. Consequently, this type of abrupt change in vegetation productivity must be built into land management strategies.

7. Discussion. In this paper I have studied pattern solutions of the Klausmeier model (1.1) for banded vegetation at large values of the slope parameter ν, when the migration speed c satisfies either $c = O_s(1)$ or $1 \ll c \ll \nu^{1/2}$ as $\nu \to \infty$. My key results are as follows:

1. For a given value of c, the largest value of the rainfall parameter A giving patterns is $\nu^{1/2} B[(c^2 + 2B - \sqrt{c^4 + 4B})/(2c)]^{1/2}$ when $c = O_s(1)$, and $\nu^{1/2} B^{3/2} c^{-1/2}$ when $1 \ll c \ll \nu^{1/2}$. As the rainfall approaches this upper limit, the amplitude of the patterns shrinks to zero. Note that I have shown in [31, 33] that the upper limit on A has the same leading order functional form whenever $1 \ll c \ll \nu$. When $c = O_s(\nu)$, there is a change in qualitative behavior: a fold develops in the branch of pattern solutions, and the homoclinic and Hopf bifurcation loci intersect, leading to a finite upper limit on c for patterns, given by $B\nu/(2 - B)$ to leading order as $\nu \to \infty$ [32].
2. For a given value of c the smallest value of the rainfall parameter A giving patterns is $\nu^{-1/2} c^{3/2} W_{\text{spike}}(+\infty; B/c^2)$ when $c = O_s(1)$, and $1.1606 c^{3/2} \nu^{-1/2}$ when $1 \ll c \ll \nu^{1/2}$. This lower limit corresponds to infinite pattern wavelength: a homoclinic (pulse) wave in (1.2). The function W_{spike} is defined in section 3. Consistency requires $W_{\text{spike}}(+\infty; \xi) \to 1.1606$ as $\xi \to 0^+$, and this is confirmed by numerical calculations (see Appendix A). Note that I showed in [33] that the lower limit on A retains the same leading order functional form up to $c = 0.8807 B^{3/4} \nu^{1/2}$, when it changes abruptly to $0.9003 B^{3/2} c^{-1/2} \nu^{1/2}$.
3. A particularly important implication of points 1 and 2 is that as c varies, patterns exist for values of the rainfall parameter A lying between $3.8405 B^{3/4} \nu^{-1/2}$ and $0.6436 B^{5/4} \nu^{1/2}$. The values of the wave speed c corresponding to these two limits are different, but both are $O_s(1)$ as $\nu \to \infty$.
4. For a given value of c satisfying $1 \ll c \ll \nu^{1/2}$, there is an abrupt change in pattern form at $A = 0.9003 \nu^{1/2} B^{3/2} c^{-1/2}$.

These are all formal results, valid to leading order for large ν. A natural area for future work is to attempt to establish them rigorously, for example using geometric singular perturbation theory [29, 30].

The different ν-scalings of the two limits in point 3 result in a large range of rainfall levels giving patterns. This is consistent with field data, which shows banded vegetation for a wide range of mean annual rainfall levels [47, 48]. The minimum rainfall level giving patterns is particularly significant because it heralds an abrupt transition from (patterned) vegetation to total desert. This is a consequence of the bistability of the patterned and unvegetated states, and has been noted previously in other mathematical models for banded vegetation [5, 16, 21, 49]. These previous studies are entirely simulation-based: a novel feature of my results is an analytical

formula for the critical rainfall level in the Klausmeier model (1.1). Of course, the simplicity of the model means that one cannot expect a quantitative agreement between this formula and field data. However, the parametric trends implied by the model can be expected to be paralleled in the field. There are no laboratory systems mimicking banded vegetation, and field experiments are difficult and expensive; therefore any such detailed prediction from a mathematical model of semiarid vegetation is valuable.

A key outstanding question for the Klausmeier model (1.1) is the stability of the patterns that I have been studying. The fact that (1.1) has patterns for a range of speeds is typical for PDEs possessing periodic traveling wave solutions. It is also typical that the periodic traveling waves are stable as solutions of the PDEs for only a subset of these speeds [50, 51, 52]. Numerical investigation confirms this for (1.1): Figure 1.2 shows the division of the A–c parameter region giving patterns into subregions containing stable and unstable cases. For this figure, I calculated the stability boundary via numerical continuation; see [37, 38] for details of the algorithm, which is implemented by the software package WAVETRAIN [35, 36]. Analytical determination of this stability boundary, even to leading order for large ν, is probably out of reach at the present time. However, some details of the curve are more accessible. In [34, section 7] I have already proved that the stability boundary touches the Hopf bifurcation locus at the Turing bifurcation point. The argument is a relatively simple one. Small amplitude expansion of the pattern solutions near the Hopf bifurcation locus shows that they are unstable except at the Turing point, and stability near that point is a consequence of the supercriticality of the Turing bifurcation. One possible avenue for future work is to attempt an extension of this approach to calculate the form of the stability boundary near the Turing point, using higher order terms in the small amplitude expansion near the Hopf bifurcation locus.

A notable feature of Figure 1.2 is that the stability boundary intersects the homoclinic locus at its turning point. Intuitively this is not surprising. At the value of A corresponding to this turning point the PDEs (1.1) undergo a bifurcation, with two homoclinic solutions existing for larger values of A and none for smaller values of A. This is strongly analogous to a saddle-node bifurcation of equilibria in ODEs, and therefore one expects one of these homoclinic solutions to be stable, with the other unstable. This is another feature that may be amenable to analytical investigation. There are results on the stability of homoclinic (pulse) waves in a number of PDEs (e.g., [53]). Typically, the spectrum consists of a continuous part that comes from the (stable) asymptotic equilibrium, and which lies in the left-hand half of the complex plane, and also a discrete part arising from the pulse itself. These discrete eigenvalues must include zero due to the neutral stability of the wave to translation; the other discrete eigenvalues determine stability. Equations (1.1) have some similarities with the FitzHugh–Nagumo equations, which also have periodic traveling waves in a region of parameter space bounded by a Hopf bifurcation locus and a "C-shaped" homoclinic locus [54, 55]. The stability of homoclinic solutions of the FitzHugh–Nagumo equations has been established for small values of one of the parameters [56, 57, 58]. It may be possible to adapt these approaches to prove that homoclinic solutions of (1.1) are stable/unstable at points above/below the turning point on the locus. If the homoclinic solution is unstable, then the nearby large period patterns are guaranteed to be unstable, but the converse does not hold. This issue has been studied in detail by previous authors [59, 60]. The discrete eigenvalue at zero in the spectrum of the homoclinic solution becomes a small loop for nearby periodic traveling waves. This loop can lie either to the right or left of the imaginary axis, implying instability or stability,

respectively. Sandstede and Scheel [60] derive conditions that distinguish these two cases, and these would have to be checked before the stability of large period patterns could be inferred from the stability of the homoclinic solutions.

Since this is the last in my series of papers on the Klausmeier model (1.1), I end with a short nontechnical summary of the work. The model contains three dimensionless ecological parameters, and investigation of patterns introduces as an additional parameter the uphill migration speed. I have shown that patterns exist for a large but finite range of this speed, and I have derived analytical formulae for the maximum and minimum values of the rainfall parameter giving patterns for speeds within this range. My formulae are valid to leading order for large values of the slope parameter, which is the ecologically relevant case because this parameter reflects the ratio of water flow downhill and plant dispersal. I have also derived the leading order forms of the pattern solutions. One notable feature of these is a sharp transition in pattern form in the interior of the parameter region giving patterns, which is significant for land management (see section 6). The basic fact that patterns exist for a range of wave speeds for given ecological parameters is also of direct practical importance, because it raises the possibility of history-dependence in pattern selection. This is confirmed by simulation-based studies of (1.1) [43, 44]. My results in the present paper and [31, 32, 33, 34] provide an analytical framework for understanding this hysteresis. The Klausmeier model is deliberately constructed as a simple representation of the complex phenomenon of vegetation dynamics in semiarid environments. This simplicity inevitably limits its predictive capability; however, it also makes possible the type of detailed mathematical study that I have undertaken. Extension of my results to more complex and realistic models for banded vegetation is an important challenge for future research.

Appendix A. In this appendix I describe my algorithm for numerical calculation of $W_{\text{spike}}(\pm\infty)$ and $(d/d\xi)W_{\text{spike}}(+\infty;\xi)$; here $W_{\text{spike}}(.)$ satisfies (3.1), and $\xi = B/c^2$. The first stage is a preliminary shooting method in which I solve (3.1) forwards in z from a point on the unstable eigenvector at $(0,0,\omega_0)$, close to the W_{spike}-axis, for a grid of values ω_0. I find that there are two different behaviors, according to the value of ω_0: either U_{spike} becomes negative along the solution trajectory, or U_{spike} becomes very large (presumably tending to infinity). These behaviors occur for ω_0 above or below a critical value for which the trajectory terminates back on the W_{spike}-axis: this is the required value $W_{\text{spike}}(-\infty;\xi)$. Therefore the solutions for my grid of ω_0 values give a preliminary estimate for $W_{\text{spike}}(-\infty;\xi)$ and hence also for $W_{\text{spike}}(+\infty;\xi)$.

My next step is to refine these estimates using a more sophisticated shooting method. For a given pair of values ω_1 and ω_2, I solve (3.1) as two different initial value problems, beginning at a point on the unstable eigenvector at $(0,0,\omega_1)$ and at a point on the stable eigenvector at $(0,0,\omega_2)$, close to the W_{spike}-axis in both cases. I solve forwards and backwards, respectively, in z_{spike}, calculating the values of U_{spike} and $dU_{\text{spike}}/dz_{\text{spike}}$ when $W_{\text{spike}} = \frac{1}{2}(\omega_1 + \omega_2)$; these values are unique since W_{spike} is an increasing function of z_{spike}. This gives two "mismatch" quantities as functions of ω_1 and ω_2. With this algorithm in place, I use a nonlinear algebraic equation solver to calculate the values of ω_1 and ω_2 at which these mismatch functions are both zero; these are the values of $W_{\text{spike}}(-\infty)$ and $W_{\text{spike}}(+\infty)$, respectively. The preliminary shooting method described in the previous paragraph gave good initial approximations for the nonlinear equation solver, enabling rapid convergence. I denote by ε the numerical error in these calculated values.

I now describe an extension of this algorithm to calculate $(d/d\xi)W_{\text{spike}}(+\infty;\xi)$. I

begin by calculating $W_{\text{spike}}(+\infty;\xi)$ numerically on a grid of ξ values. I then estimate the second derivative $(d^2/d\xi^2)W_{\text{spike}}(+\infty;\xi)$ at each of these grid points by quadratic interpolation through successive triples of points on the grid. For each value of ξ on the grid, I then calculate the first derivative using

$$\text{(A.1)} \quad \tfrac{d}{d\xi}W_{\text{spike}}(+\infty;\xi) \approx \left[W_{\text{spike}}\big(+\infty;\xi+h(\xi)\big) - W_{\text{spike}}\big(+\infty;\xi-h(\xi)\big)\right]/2h(\xi),$$

$$\text{(A.2)} \quad \text{where } h(\xi) = \varepsilon^{1/3}\, W_{\text{spike}}(+\infty;\xi)/\tfrac{d^2}{d\xi^2}W_{\text{spike}}(+\infty;\xi)\,.$$

The spacing (A.2) is an optimal choice for the numerical estimation of the first derivative and gives an error in the numerical derivative of about $\varepsilon^{2/3}$ [61, section 5.7].

The numerical errors in the values given by this algorithm for $W_{\text{spike}}(+\infty;\xi)$ and $(d/d\xi)W_{\text{spike}}(+\infty;\xi)$ depend on three tolerances: the distance ρ from the W_{spike}-axis of the point on the unstable eigenvector of (3.1) along which shooting is started, the local error tolerance ℓ of the ODE solver, and the absolute error tolerance τ in the nonlinear equation solver used to calculate $W_{\text{spike}}(\pm\infty;\xi)$. I consider first the optimal choice of ρ. For a given point $(0,0,\omega_0)$, I denote by λ and $\underline{E}$ the unstable eigenvalue of (3.1) and the corresponding normalized eigenvector; both of these are real, and $E_3 = 0$. Then the starting point for numerical solution of (3.1) is $(U_{\text{spike}}, V_{\text{spike}}, W_{\text{spike}})|_{z_{\text{spike}}=0} = (0,0,\omega_0) + \rho\underline{E}$. After a few numerical integration steps, the first two components of the numerical solution are

$$(U_{\text{spike}}, V_{\text{spike}}) = \rho\exp\{\lambda z_{\text{spike}}\}(E_1,E_2) + \ell\underline{\mathcal{L}}(z_{\text{spike}}) + \rho^2\underline{\mathcal{R}}(z_{\text{spike}}),$$

where $\underline{\mathcal{L}}$, $\underline{\mathcal{R}} \in \mathbb{R}^2$ are $O(1)$ as ℓ, $\rho \to 0$. The ρ^2 term arises from nonlinear terms in the ODEs. The deviation of this point from the eigenvector is given by

$$\frac{\rho E_1\exp\{\lambda z_{\text{spike}}\} + \ell\mathcal{L}_1(z_{\text{spike}}) + \rho^2\mathcal{R}_1(z_{\text{spike}})}{\rho E_2\exp\{\lambda z_{\text{spike}}\} + \ell\mathcal{L}_2(z_{\text{spike}}) + \rho^2\mathcal{R}_2(z_{\text{spike}})} - \frac{\rho E_1\exp\{\lambda z_{\text{spike}}\}}{\rho E_2\exp\{\lambda z_{\text{spike}}\}},$$

which is $O(\rho+\ell/\rho)$ as $\ell,\rho \to 0$. To minimize this deviation, I therefore chose $\rho = \sqrt{\ell}$, and I ran tests to confirm the optimality of this choice.

In addition to λ (> 0), there are two other eigenvalues of (3.1) at $(0,0,\omega_0)$: one negative, with the eigenvector again lying in the U_{spike}–V_{spike} plane, and the other zero, with eigenvector $(0,0,1)$. Therefore the U_{spike} and V_{spike} components of the numerical solution gradually return to those of the required solution trajectory, but the error caused by deviation from the eigenvector persists in the W_{spike} component of the solution. However, the form of (3.1c) implies that this error is $O(\ell^{3/2})$, and it is therefore dominated by local errors in the ODE solution.

Since the number of steps in the numerical solution of (3.1) is not particularly large, these various considerations imply that the global error in the solution is $O(\ell)$. Provided that τ is chosen significantly smaller than ℓ, it follows that $\varepsilon = O(\ell)$. Hence the numerical errors in $W_{\text{spike}}(+\infty;\xi)$ and $(d/d\xi)W_{\text{spike}}(+\infty;\xi)$ are $O(\ell)$ and $O(\ell^{2/3})$, respectively. I chose $\ell = 10^{-8}$ using 8-byte precision, giving error estimates of 10^{-8} and 5×10^{-6}, respectively.

Finally I comment on the numerical estimation of $\lim_{\xi\to0^+} W_{\text{spike}}(+\infty;\xi)$. Since $B/c^2 \to 0$ is a singular limit for (3.1) (see Figure 6.1 and associated discussion), numerical calculation of $W_{\text{spike}}(+\infty;\xi)$ becomes progressively more difficult as ξ is decreased towards zero, and the algorithm ultimately fails. Therefore I estimated the limiting value by fitting a polynomial through a sequence of values for small nonzero ξ. This gives the limit as 1.1606, which is consistent with the calculations in section 6.

Acknowledgments. I am grateful to Markus Bär and Arnd Scheel for helpful discussions concerning the stability of homoclinic solutions.

REFERENCES

[1] R. M. CALLAWAY, *Positive interactions among plants*, Botanical Rev., 61 (1995), pp. 306–349.
[2] M. RIETKERK, P. KETNER, J. BURGER, B. HOORENS, AND H. OLFF, *Multiscale soil and vegetation patchiness along a gradient of herbivore impact in a semi-arid grazing system in West Africa*, Plant Ecol., 148 (2000), pp. 207–224.
[3] M. R. AGULAR AND O. E. SALA, *Patch structure, dynamics and implications for the functioning of arid ecosystems*, Trends Ecol. Evol., 14 (1999), pp. 273–277.
[4] C. VALENTIN, J. M. D'HERBÈS, AND J. POESEN, *Soil and water components of banded vegetation patterns*, Catena, 37 (1999), pp. 1–24.
[5] M. RIETKERK, S. C. DEKKER, P. C. DE RUITER, AND J. VAN DE KOPPEL, *Self-organized patchiness and catastrophic shifts in ecosystems*, Science, 305 (2004), pp. 1926–1929.
[6] D. L. DUNKERLEY AND K. J. BROWN, *Oblique vegetation banding in the Australian arid zone: Implications for theories of pattern evolution and maintenance*, J. Arid Environ., 52 (2002), pp. 163–181.
[7] A. K. MCDONALD, R. J. KINUCAN, AND L. E. LOOMIS, *Ecohydrological interactions within banded vegetation in the northeastern Chihuahuan Desert, USA*, Ecohydrol., 2 (2009), pp. 66–71.
[8] P. COUTERON, A. MAHAMANE, P. OUEDRAOGO, AND J. SEGHIERI, *Differences between banded thickets (tiger bush) at two sites in West Africa*, J. Veg. Sci., 11 (2000), pp. 321–328.
[9] C. MONTAÑA, J. SEGHIERI, AND A. CORNET, *Vegetation dynamics: Recruitment, regeneration in two-phase mosaics*, in Banded Vegetation Patterning in Arid and Semiarid Environments, D. J. Tongway, C. Valentin, and J. Seghieri, eds., Springer, New York, 2001, pp. 132–145.
[10] D. J. TONGWAY AND J. A. LUDWIG, *Theories on the origins, maintenance, dynamics, and functioning of banded landscapes*, in Banded Vegetation Patterning in Arid and Semiarid Environments, D. J. Tongway, C. Valentin, and J. Seghieri, eds., Springer, New York, 2001, pp. 20–31.
[11] V. DEBLAUWE, P. COUTERON, J. BOGAERT, AND N. BARBIER, *Determinants and dynamics of banded vegetation pattern migration in arid climates*, Ecol. Monogr., 82 (2012), pp. 3–21.
[12] P. M. SACO, G. R. WILLGOOSE, AND G. R. HANCOCK, *Eco-geomorphology of banded vegetation patterns in arid and semi-arid regions*, Hydrol. Earth Syst. Sci., 11 (2007), pp. 1717–1730.
[13] S. THOMPSON AND G. KATUL, *Secondary seed dispersal and its role in landscape organization*, Geophys. Res. Lett., 36 (2009), L02402.
[14] C. A. KLAUSMEIER, *Regular and irregular patterns in semiarid vegetation*, Science, 284 (1999), pp. 1826–1828.
[15] N. BARBIER, P. COUTERON, R. LEFEVER, V. DEBLAUWE, AND O. LEJEUNE, *Spatial decoupling of facilitation and competition at the origin of gapped vegetation patterns*, Ecology, 89 (2008), pp. 1521–1531.
[16] E. GILAD, J. VON HARDENBERG, A. PROVENZALE, M. SHACHAK, AND E. MERON, *A mathematical model of plants as ecosystem engineers*, J. Theoret. Biol., 244 (2007) pp. 680–691.
[17] J. VON HARDENBERG, A. Y. KLETTER, H. YIZHAQ, J. NATHAN, AND E. MERON, *Periodic versus scale-free patterns in dryland vegetation*, Proc. R. Soc. Lond. Ser. B, 277 (2010), pp. 1771–1776.
[18] R. LEFEVER AND O. LEJEUNE, *On the origin of tiger bush*, Bull. Math. Biol., 59 (1997), pp. 263–294.
[19] R. LEFEVER, N. BARBIER, P. COUTERON, AND O. LEJEUNE, *Deeply gapped vegetation patterns: On crown/root allometry, criticality and desertification*, J. Theoret. Biol., 261 (2009), pp. 194–209.
[20] J. A. SHERRATT, *An analysis of vegetation stripe formation in semi-arid landscapes*, J. Math. Biol., 51 (2005), pp. 183–197.
[21] J. VON HARDENBERG, E. MERON, M. SHACHAK, AND Y. ZARMI, *Diversity of vegetation patterns and desertification*, Phys. Rev. Lett., 87 (2001), 198101.
[22] M. RIETKERK, M. C. BOERLIJST, F. VAN LANGEVELDE, R. HILLERISLAMBERS, J. VAN DE KOPPEL, H. H. T. PRINS, AND A. DE ROOS, *Self-organisation of vegetation in arid ecosystems*, Am. Nat., 160 (2002), pp. 524–530.
[23] N. URSINO, *Above and below ground biomass patterns in arid lands*, Ecolog. Model., 220 (2009), pp. 1411–1418.

[24] J. VAN DE KOPPEL, M. RIETKERK, F. VAN LANGEVELDE, L. KUMAR, C. A. KLAUSMEIER, J. M. FRYXELL, J. W. HEARNE, J. VAN ANDEL, N. DE RIDDER, M. A. SKIDMORE, L. STROOSNIJDER, AND H. H. T. PRINS, *Spatial heterogeneity and irreversible vegetation change in semiarid grazing systems*, Am. Nat., 159 (2002), pp. 209–218.

[25] N. URSINO AND S. CONTARINI, *Stability of banded vegetation patterns under seasonal rainfall and limited soil moisture storage capacity*, Adv. Water Resour., 29 (2006), pp. 1556–1564.

[26] V. GUTTAL AND C. JAYAPRAKASH, *Self-organisation and productivity in semi-arid ecosystems: Implications of seasonality in rainfall*, J. Theoret. Biol., 248 (2007), pp. 290–500.

[27] A. Y. KLETTER, J. VON HARDENBERG, E. MERON, AND A. PROVENZALE, *Patterned vegetation and rainfall intermittency*, J. Theoret. Biol., 256 (2009), pp. 574–583.

[28] Y. GOTO, D. HILHORST, E. MERON, AND R. TEMAM, *Existence theorem for a model of dryland vegetation*, Discrete Contin. Dyn. Syst. B, 16 (2011), pp. 197–224.

[29] C. K. R. T. JONES, *Geometric singular perturbation theory*, in Dynamical Systems, R. Johnson, ed., Lecture Notes in Math. 1609, Springer-Verlag, Berlin, 1995, pp. 44–118.

[30] P. VAN HEIJSTER AND B. SANDSTEDE, *Planar radial spots in a three-component FitzHugh-Nagumo system*, J. Nonlinear Sci., 21 (2011), pp. 705–745.

[31] J. A. SHERRATT, *Pattern solutions of the Klausmeier model for banded vegetation in semi-arid environments* I, Nonlinearity, 23 (2010), pp. 2657–2675.

[32] J. A. SHERRATT, *Pattern solutions of the Klausmeier model for banded vegetation in semi-arid environments* II: *Patterns with the largest possible propagation speeds*, Proc. R. Soc. Lond. Ser. A, 467 (2011), pp. 3272–3294.

[33] J. A. SHERRATT, *Pattern solutions of the Klausmeier model for banded vegetation in semi-arid environments* III: *The transition between homoclinic solutions*, Phys. D, 242 (2013), pp. 30–41.

[34] J. A. SHERRATT, *Pattern solutions of the Klausmeier model for banded vegetation in semiarid environments* IV: *Slowly moving patterns and their stability*, SIAM J. Appl. Math., 73 (2013), pp. 330–350.

[35] J. A. SHERRATT, *Numerical continuation methods for studying periodic travelling wave (wavetrain) solutions of partial differential equations*, Appl. Math. Comput., 218 (2012), pp. 4684–4694.

[36] J. A. SHERRATT, *WAVETRAIN: Free, Open-Source Software for Studying Periodic Travelling Wave Solutions of Partial Differential Equations*, online at http://www.ma.hw.ac.uk/wavetrain.

[37] J. A. SHERRATT, *Numerical continuation of boundaries in parameter space between stable and unstable periodic travelling wave (wavetrain) solutions of partial differential equations*, Adv. Comput. Math., 39 (2013), pp. 175–192.

[38] J. D. M. RADEMACHER, B. SANDSTEDE, AND A. SCHEEL, *Computing absolute and essential spectra using continuation*, Phys. D, 229 (2007), pp. 166–183.

[39] E. J. DOEDEL, *AUTO, A program for the automatic bifurcation analysis of autonomous systems*, Cong. Numer., 30 (1981), pp. 265–384.

[40] E. J. DOEDEL, H. B. KELLER, AND J. P. KERNÉVEZ, *Numerical analysis and control of bifurcation problems:* (I) *Bifurcation in finite dimensions*, Internat. J. Bifur. Chaos Appl. Sci. Engrg., 1 (1991), pp. 493–520.

[41] E. J. DOEDEL, W. GOVAERTS, Y. A. KUZNETSOV, AND A. DHOOGE, *Numerical continuation of branch points of equilibria and periodic orbits*, in Modelling and Computations in Dynamical Systems, E. J. Doedel, G. Domokos, and I. G. Kevrekidis, eds., World Scientific, River Edge, NJ, 2006, pp. 145–164.

[42] A. I. BORTHAGARAY, M. A. FUENTES, AND P. A. MARQUET, *Vegetation pattern formation in a fog-dependent ecosystem*, J. Theoret. Biol., 265 (2010), pp. 18–26.

[43] J. A. SHERRATT AND G. J. LORD, *Nonlinear dynamics, pattern bifurcations in a model for vegetation stripes in semi-arid environments*, Theor. Popul. Biol., 71 (2007), pp. 1–11.

[44] J. A. SHERRATT, *History-dependent patterns of whole ecosystems*, Ecol. Complex., 14 (2013), pp. 8–20.

[45] D. O. FREUDENBERGER AND P. HIERNAUX, *Productivity of patterned vegetation*, in Banded Vegetation Patterning in Arid and Semiarid Environments, D. J. Tongway, C. Valentin, and J. Seghieri, eds., Springer, New York, 2001, pp. 198–209.

[46] J. C. NOBLE, R. PELTIER, P. MONTAGNE, AND EL E. H. MAHAMANE, *Toward improved management of arid and semiarid banded landscapes*, in Banded Vegetation Patterning in Arid and Semiarid Environments, D. J. Tongway, C. Valentin, and J. Seghieri, eds., Springer, New York, 2001, pp. 210–227.

[47] C. VALENTIN AND J. M. D'HERBÈS, *Niger tiger bush as a natural water harvesting system*, Catena, 37 (1999), pp. 231–256.

[48] V. DEBLAUWE, N. BARBIER, P. COUTERON, O. LEJEUNE, AND J. BOGAERT, *The global biogeography of semi-arid periodic vegetation patterns*, Global Ecol. Biogeography, 17 (2008), pp. 715–723.

[49] E. MERON, *Pattern-formation approach to modelling spatially extended ecosystems*, Ecolog. Model., 234 (2012), pp. 70–82.

[50] N. KOPELL AND L. N. HOWARD, *Plane wave solutions to reaction-diffusion equations*, Stud. Appl. Math., 52 (1973), pp. 291–328.

[51] K. MAGINU, *Stability of periodic travelling wave solutions with large spatial periods in reaction-diffusion systems*, J. Differential Equations, 39 (1981), pp. 73–99.

[52] J. A. SHERRATT AND M. J. SMITH, *Periodic travelling waves in cyclic populations: Field studies and reaction-diffusion models*, J. R. Soc. Interface, 5 (2008), pp. 483–505.

[53] R. L. PEGO AND M. I. WEINSTEIN, *Eigenvalues, and instabilities of solitary waves*, Phil. Trans. R. Soc. A, 340 (1992), pp. 47–94.

[54] M. KRUPA, B. SANDSTEDE, AND P. SZMOLYAN, *Fast and slow waves in the FitzHugh-Nagumo equation*, J. Differential Equations, 133 (1997), pp. 49–97.

[55] A. R. CHAMPNEYS, V. KIRK, E. KNOBLOCH, B. E. OLDEMAN, AND J. SNEYD, *When Shil'nikov meets Hopf in excitable systems*, SIAM J. Appl. Dyn. Syst., 6 (2007), pp. 663–693.

[56] C. K. R. T. JONES, *Stability of the travelling wave solution of the Fitzhugh-Nagumo system*, Trans. Amer. Math. Soc., 286 (1984), pp. 431–469.

[57] E. YANAGIDA, *Stability of fast traveling pulse solutions of the Fitzhugh-Nagumo equations*, J. Math. Biol., 22 (1985), pp. 81–104.

[58] G. FLORES, *Stability analysis for the slow traveling pulse of the FitzHugh–Nagumo system*, SIAM J. Math. Anal., 22 (1991), pp. 392–399.

[59] R. GARDNER, *Spectral analysis of long wavelength periodic waves and applications*, J. Reine Angew. Math., 491 (1997), pp. 149–181.

[60] B. SANDSTEDE AND A. SCHEEL, *On the stability of periodic travelling waves with large spatial period*, J. Differential Equations, 172 (2001), pp. 134–188.

[61] W. H. PRESS, S. A. TEUKOLSKY, W. T. VETTERLING, AND B. P. FLANNERY, *Numerical Recipes: The Art of Scientific Computing*, 3rd ed., Cambridge University Press, Cambridge, UK, 2007.